Ionics
https://doi.org/10.1007/s11581-025-06486-9

RESEARCH

Porous structure of Fe_2O_3 thin films prepared for supercapacitors via CBD method: effect of molar concentration

A. A. Admuthe[1] · P. A. Desai[2] · S. G. Pawar[3] · S. L. Jadhav[4] · A. L. Jadhav[4] · D. B. Malavekar[5] · N. S. Bachankar[5] · J. H. Kim[5] · K. V. Gaikwad[6] · V. S. Jamadade[1]

Received: 19 April 2025 / Revised: 28 May 2025 / Accepted: 14 June 2025

Abstract

In present study, iron oxide (Fe_2O_3) thin films were fabricated using a simple chemical bath deposition method, and the effect of precursor concentration (0.05 M, 0.1 M and 0.15 M) on the electrochemical properties was investigated. The X-ray diffraction analysis confirmed that the hematite (Fe_2O_3) phase of material, while water contact angle measurements revealed a hydrophilic nature. The scanning electron microscopy images exhibited a random distribution of porous structures, with a uniform coating and rough grain morphology. The energy-dispersive X-ray spectroscopy further confirmed the presence of iron (Fe) and oxygen (O) elements in the films. Brunauer–Emmett–Teller (BET) surface area analysis showed 41.19 $m^2\ g^{-1}$ of specific surface area for Fe_2O_3 thin film deposited using 0.15 M precursor. The electrochemical performance of the films was evaluated for charge storage applications, with cyclic voltammetry revealing a high specific capacitance of 495 F g^{-1} at a scan rate of 5 mV s^{-1} for 0.15 M precursor concentration in 1 M NaOH electrolyte. Galvanostatic charge–discharge measurements confirmed a specific capacitance of 337 F g^{-1} at a current density of 3.1 A g^{-1}. These findings suggest that Fe_2O_3 thin films deposited at optimized concentration of iron precursor exhibit significant potential as candidates for supercapacitor applications.

Keywords Iron oxide · Chemical bath deposition · Energy storage · Specific capacitance · Supercapacitor

Introduction

The demand for energy has significantly increased due to the advancement of humanity. However, conventional energy production methods are contributing to serious environmental challenges and climate change. The growing urgency for clean and sustainable energy sources can only be addressed through the utilization of renewable energy. Despite this, certain renewable energy sources are intermittent, which poses a challenge to their reliability over extended period [1]. It is crucial to develop renewable, non-conventional energy sources and establish an efficient energy storage system that can operate coherently. In other words, there is a need to transition from traditional, reliable energy collectors to more efficient, rapid and sustainable power storage solutions. Energy storage is becoming a more important research topic in the present work [2, 3]. The fabrication and synthesis of suitable materials exhibiting high power density and charge/discharge rate in addition to the longer life cycle and environmental favourable are the current research focus among material scientists [4, 5]. Also, Supercapacitors have gained significant attention due to their advantages, including portability, lightweight design, rapid charging capabilities, and high cyclic stability [6, 7]. Given these advantages, extensive research has been dedicated to the development

✉ V. S. Jamadade
vinayakjamadade@gmail.com

1 Department of Physics, D.P. Bhosale College, Koregaon (Satara), India

2 Department of Physics, Smt. K.R.P. Kanya Mahavidyalaya, Uran Islampur, India

3 Department of Physics, D.B.F. Dayanand College of Arts and Science, Solapur, India

4 The Institute of Science, Dr. Homi Bhabha State University, Mumbai, India

5 Department of Material Science and Engineering, Optoelectronic Convergence Research Center, Chonnam National University Gwangju, Gwangju, South Korea

6 Department of Chemistry, R. C. Shahu College, Kolhapur, India

Published online: 21 June 2025

of advanced materials for supercapacitor electrodes, aimed at enhancing rapid electron transfer and optimizing charge storage capabilities [8, 9].

On the basis of charge storage mechanisms, electrochemical supercapacitors are classified into two types, electrical double-layer capacitors (EDLCs) and pseudocapacitors. Through the adsorption process, EDLCs can store charge in an electrostatic way, which is located at the electrode/electrolyte interface [10]. The pseudocapacitors store charges following simultaneous faradic reactions at the electrode surface. Consequently, the pseudocapacitor contains higher specific capacitance (SC) than the EDLC type [11].

Numerous materials have been explored and studied as electrode materials for supercapacitors, including carbon allotropes offer advantages such as higher stability and power density. Owing to the EDLCs storage mechanism of, carbon materials can provide high power density, but less energy density, which limits all over performance. Carbon materials such as carbon nanotubes, graphene, and carbon nanofibers have been studied for electrode materials but carbon materials are limited by their very high cost. In the preceding decade, major efforts have been made developing a hybrid supercapacitor to accomplish the demands of high energy density and high power density [12]. Conversely, pseudocapacitive materials offer greater energy density but fall short in terms of cycling stability. Hence, developing new materials that can effectively balance both energy storage capacity and long-term stability is essential for advancing supercapacitor performance [13].

In contrast, metal oxides are known to achieve higher energy densities [14, 15]. Various transition metal oxides, RuO_2, MnO_2, Co_3O_4, SnO_2, IrO_2, NiO, iron oxide (Fe_2O_3), have been investigated for supercapacitor application [16, 17]. Among these, RuO_2 is particularly favored due to its high specific capacitance and long cycle life. However, RuO_2 is expensive, toxic, and challenging to produce in large quantities, limiting its practical use.

In this regard, Fe_2O_3, a low-cost and environmentally friendly material, has been proposed as an alternative negative electrode for supercapacitors in aqueous electrolytes [18, 19]. Despite its potential, iron oxide suffers from inherent limitations, such as poor electrical conductivity, limited active surface area, and reduced charge storage efficiency after extended operation, which hinders its practical ability to deliver high specific capacitance [20]. There are previous efforts to improve the capacity of the iron oxide. These include development of the composite material, self-supported material, doping, and morphology engineering, etc. For example, Sohouli et al. [21] prepared composite of carbon, MnO_2 and Fe_3O_4 that can deliver specific capacitance of 730 F g^{-1} at a 4 A g^{-1}. Kumar et al. [22] prepared reduced graphene oxide composite with Fe_3O_4, delivering specific capacitance of 771.3 F g^{-1} at a scan rate of 5 mV s^{-1}. These studies underscore the applicability of iron oxide in the supercapacitive charge storage.

In the present work, we report development of self-supported Fe_2O_3-based electrode for supercapacitor using chemical bath deposition (CBD) method on stainless steel (SS) conductive support. The novelty of this work lies in the use of ferrous sulfate heptahydrate and sodium hydroxide as precursors for the synthesis of iron oxide thin films via chemical bath deposition (CBD), with a particular focus on the effect of molar concentration on film properties and supercapacitor performance. Limited research has investigated how variations in precursor molarity, especially using this specific combination in the CBD method, influence film morphology, phase composition, and electrochemical behavior. This study provides valuable insights into the tunability of iron oxide film characteristics through a simple and cost-effective chemical approach, highlighting its impact on capacitance and cycling stability.

The synthesized Fe_2O_3 thin film electrodes were characterized using X-ray diffraction (XRD), scanning electron micrographs (SEM), energy dispersive of X-ray (EDAX), contact angle measurements, and Brunauer–Emmett–Teller (BET) analysis. Furthermore, the supercapacitive performance was evaluated using cyclic voltammetry (CV), galvanostatic charge–discharge (GCD), and electrochemical impedance spectroscopy (EIS). The Fe_2O_3 thin film electrode showed a maximum value of specific capacitance of 495 F g^{-1} at a scan rate of 5 mV s^{-1}.

Experimental details

Materials

Analytical grade chemicals, including ferrous sulfate heptahydrate ($FeSO_4 \cdot 7H_2O$, purity ≥ 99%, Sigma Alrich) and sodium hydroxide (NaOH, purity ≥ 98%, Sigma Alrich), were used in experiments. Double distilled water (DDW) was used as the solvent. Well-polished SS substrates (304 grade) of thickness 0.7 mm were used for the deposition of thin films. The SS substrates were procured from local market.

Synthesis of Fe_2O_3 thin film

Self-supported Fe_2O_3 thin film electrodes were deposited using the CBD method. The SS substrates were first polished with zero-grade abrasive paper, followed by cleaning with labolene (used as a detergent), and thoroughly rinsed with DDW. After rinsing, the substrates were sonicated in DDW for 15 min to ensure complete removal of contaminants on the surface. The cleaned SS substrates

were then used for thin film deposition. $FeSO_4 \cdot 7H_2O$ was used as the iron ion source for the deposition process. To prepare the Fe_2O_3 thin films, aqueous ferrous sulfate solutions of 0.05 M, 0.1 M, and 0.15 M concentrations were prepared in 50 mL of DDW. To each solution, 1 M NaOH was added to maintain the pH at 8. This solution was stirred for 10 min and heated up to 85°. After 30 min, the solution turned blackish in color, indicating the onset of film formation. At this stage, the SS substrates were immersed in the solution for 30 min, resulting in the formation of uniform and well-adhered Fe_2O_3 thin films on the substrate surface. The deposited films were withdrawn from flask at appropriate intervals, rinsed with DDW, and dried in furnace at 150° for 1 h, and subjected to characterize for supercapacitive performance. The 1 M aqueous solution of NaOH as an electrolyte used for the study of different molarities Fe_2O_3 thin films.

Figure 1 shows the mass loading of thin films deposited with varying molarities. The mass loading of Fe_2O_3 thin films was measured to be 0.00029, 0.00033, 0.00026 g cm^{-2} for precursor concentrations of 0.05 M, 0.1 M and 0.15 M, respectively. An increase in precursor concentration enhances ion availability, resulting in higher deposition and therefore, the 0.00026 g cm^{-2} mass loading increases up to 0.00033 g cm^{-2} for 0.1 M thin film. However, at higher concentrations (0.15 M), the formation of larger particles due to rapid nucleation leads to non-uniform deposition, thereby reducing the film thickness. For precursor concentrations of 0.05 M, 0.1 M and 0.15 M, the corresponding film thickness were approximately 553.4 nm, 629.8 nm, and 496.2 nm, respectively. The calculations were performed considering the density of Fe_2O_3 as 5.2 g cm^{-3}.

Characterizations

The phase of the prepared Fe_2O_3 thin films on SS substrates was determined using XRD analysis, performed with a Bruker D2 Phaser X-ray diffractometer (United States) operating with a Cu Kα X-ray source (λ = 1.54 Å). The contact angle (CA) measurements were performed using a goniometer to observe the interaction between Fe_2O_3 thin films and water. The SEM micrographs were taken to observe the topography of deposited films using SEM, (JEOL JSM-IT200, Japan). The EDAX was performed to get elemental spectra. The BET measurements were performed using Quantach-rome Instruments v11.02. To evaluate the supercapacitive properties, CV and GCD measurements of the Fe_2O_3 thin film electrodes were conducted within a potential window of −1.2 V to −0.4 V in a 1 M NaOH electrolyte. A platinum sheet with an area of 1 cm^2 was used as the counter electrode, while an Ag/AgCl electrode (1 M NaCl) served as the reference electrode. The EIS was employed to assess the charge transfer properties of the electrodes, and the stability of the electrodes was evaluated by performing CV measurements over 1000 cycles.

Results and discussion

Thin film formation

Fe_2O_3 thin films were deposited on SS substrates using the CBD method. The formation of the thin film is initiated through heterogeneous nucleation, followed by particle growth [23]. Upon the addition of NaOH to the precursor solution, precipitation was induced. To control particle growth, additional

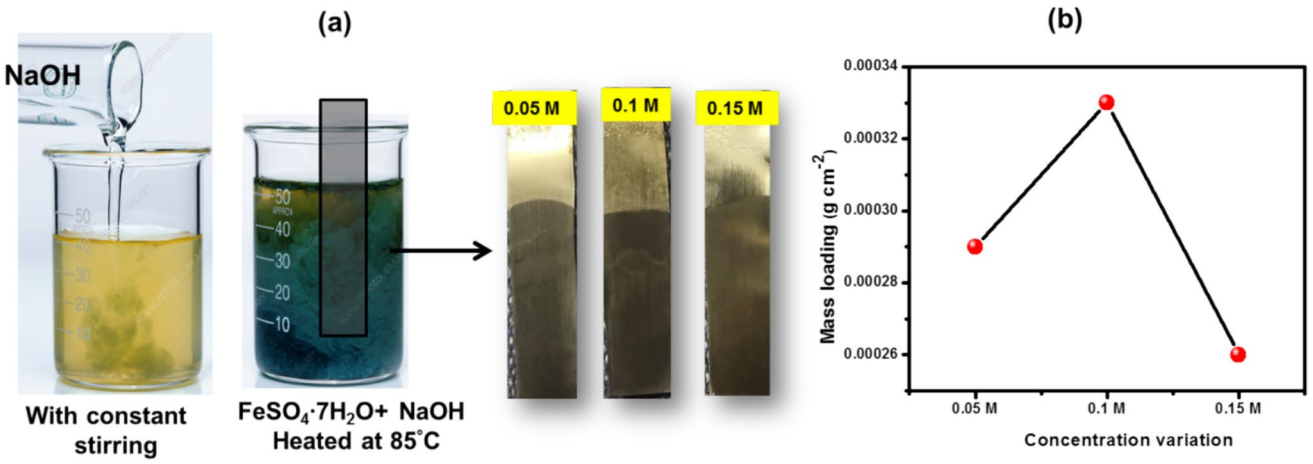

Fig. 1 **a)** Schematic illustration of Fe_2O_3 thin films using CBD method with the photograph of Fe_2O_3 thin films deposited with varying molarities of iron ion source, and **b)** variation of mass loading for Fe_2O_3 thin films

NaOH was added until the pH of the solution reached 8. The following relations describe the chemical reactions:

$$Fe_2(SO_4)_3 + 6NaOH \rightarrow 2Fe(OH)_3 + 3Na_2SO_4 \quad (1)$$

After annealing at a temperature of 150℃ in the air,

$$2Fe(OH)_3 \rightarrow Fe_2O_3 + 3H_2O \quad (2)$$

Structural analysis

The structural properties of the prepared thin film materials were investigated using XRD. The XRD patterns of the deposited thin films are shown in Fig. 2. Two prominent diffraction peaks, corresponding to the (104) and (110) crystal planes, were observed, confirming the formation of Fe_2O_3. These peaks are consistent with the JCPDS card number #72–0469. Three additional peaks were attributed to the SS substrate. It was observed that the intensity of the (110) peak increased as the precursor concentration varied from 0.05 M to 0.15 M, indicating an improvement in the crystallinity of the Fe_2O_3 layer. However, a further increase in the precursor concentration to 0.15 M resulted in a reduction in crystallinity. This suggests that the optimal crystallinity was achieved at a precursor concentration of 0.1 M. The structural parameters of the Fe_2O_3 thin films, including microstrain (ε), dislocation density (σ), and stacking fault (S.F.), were calculated using the following relations: [24],

$$\sigma = \frac{1}{D^2} \quad (3)$$

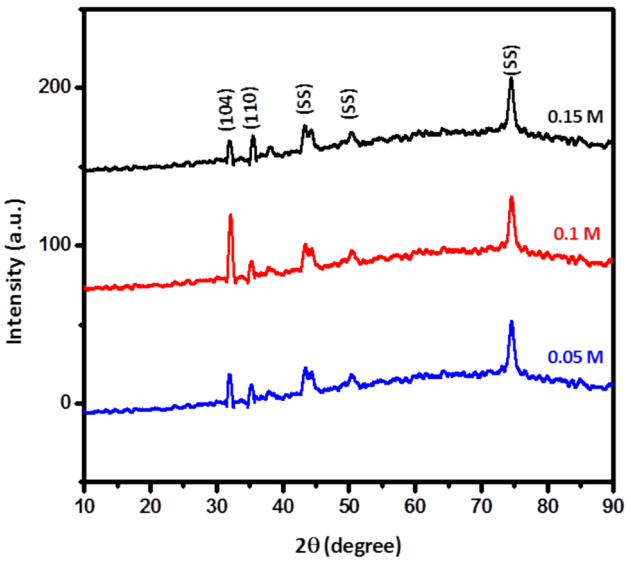

Fig. 2 X-ray diffraction study of different molarities of Fe_2O_3 films on SS substrate

$$\varepsilon = \frac{\beta \cos\theta}{4} \quad (4)$$

$$S.F. = \frac{2\pi^2}{45(3tan\theta)^{1/2}}\beta \quad (5)$$

$$D = \frac{0.9\lambda}{\beta \cos\theta} \quad (6)$$

The microstructural results for the different samples (0.05 M, 0.1 M, and 0.15 M) are summarised in Table 1. As shown in Table 1, the values of σ, ε, and S.F. decrease with increasing precursor concentration from 0.05 M to 0.1 M. However, at a precursor concentration of 0.15 M, an increase in σ, ε, and S.F. is observed. This behaviour can be attributed to the reduced film thickness at 0.15 M compared to the 0.05 M and 0.1 M concentrations of iron precursor. These findings suggest that a lower crystallite size leads to an increase in the defect level [25, 26]. The density of dislocations can influence the overall capacitance of the supercapacitor. A higher dislocation density in the electrode material may enhance the effective surface area, potentially increasing the capacitance. Regarding stacking faults, these defects can alter the ionic and electronic transport properties of the material, affecting the rate capability of the supercapacitor [27]. An increased number of stacking faults may improve the charge/discharge kinetics. Furthermore, microstrain can increase the specific surface area, thereby improving the supercapacitive performance.

Morphological study (SEM)

The morphological characteristics of Fe_2O_3 films deposited at different precursor concentrations were analyzed, and the corresponding SEM images at various magnifications are shown in Fig. 3. The SEM micrographs reveal that the surface morphology of the material is highly dependent on precursor concentration. For the Fe_2O_3 thin films, the electrode surface is well-covered with smooth and irregularly shaped particles. These interconnected particles highlight the influence of precursor concentration on the nucleation process. As the molarity of the

Table 1 Micro-structural parameters for Fe_2O_3 thin films deposited on SS substrate

Samples	Crystallite size (nm)	Dislocation density (σ) $(cm^{-2}) \times 10^{-3}$	Microstrain (ε)	Stacking fault
0.05 M	15.75	4.031	0.1260	0.2473
0.1 M	16.51	3.668	0.1201	0.2359
0.15 M	14.49	4.762	0.1381	0.2710

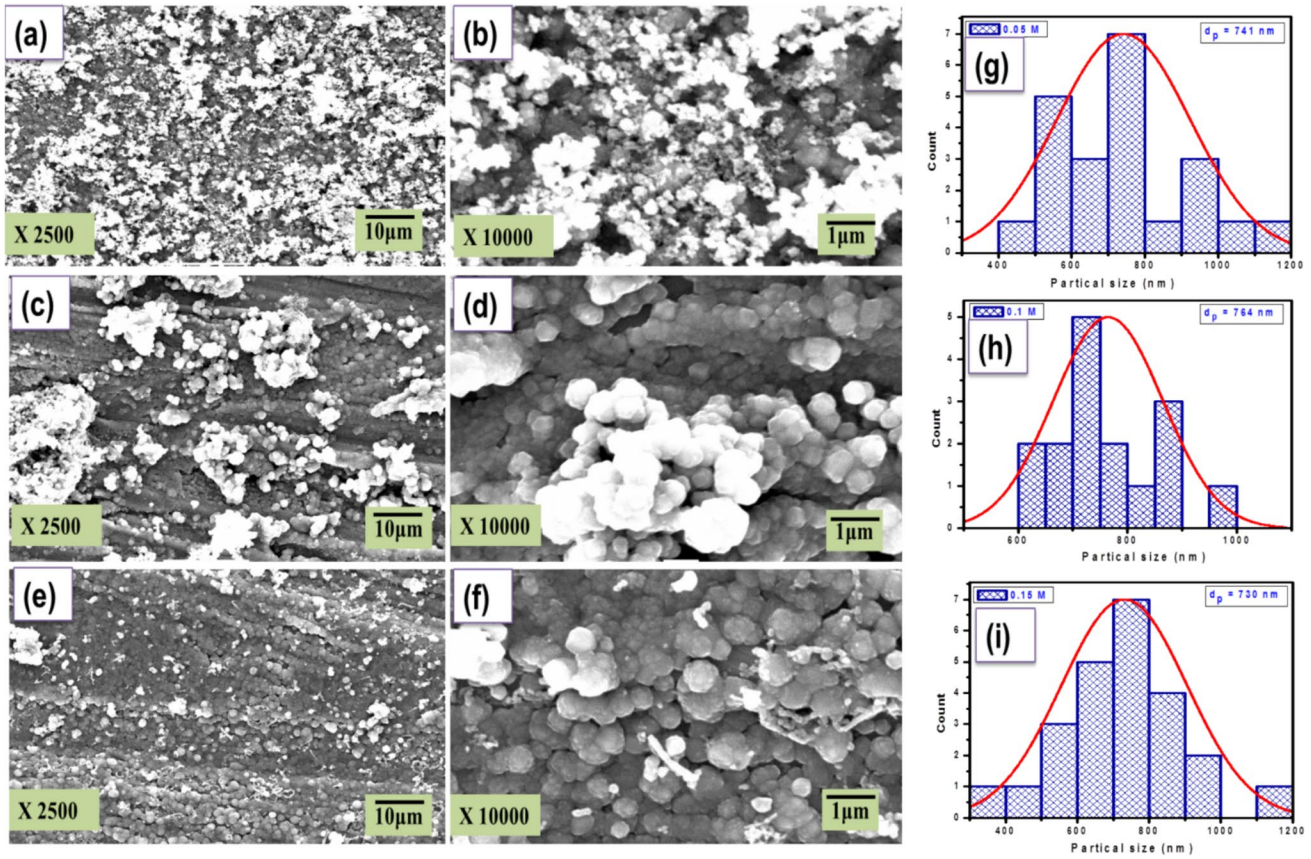

Fig. 3 The SEM micrographs of Fe_2O_3 film deposited at different concentrations of iron precursors **a, b)** 0.05 M, **c, d)** 0.1 M, and **e, f)** 0.15 M at different magnifications of 2500X and 10000X. The particle size distribution of Fe_2O_3 film deposited at different concentrations of iron precursors **g)** 0.05 M, **h)** 0.1 M, and **i)** 0.15 M

precursor increases from 0.05 M to 0.15 M, the grain size increases due to the closer proximity of the grains. However, the hematite (Fe_2O_3) nanoparticles exhibit high surface energy owing to their large surface area, which promotes agglomeration and the formation of clusters [28]. The interconnected nature of the particles facilitates the rapid movement of electrons within the material, leading to faster charge and discharge rates. This characteristic enables the supercapacitors to deliver high power outputs. The average particle sizes for the films prepared with precursor concentrations of 0.05 M, 0.1 M, and 0.15 M were approximately 741 nm, 764 nm, and 730 nm, respectively, as estimated from SEM image analysis. These values indicate that the particle size slightly increases with increasing concentration up to 0.1 M, but decreases at 0.15 M, suggesting improved nucleation and growth control at higher concentrations. The corresponding particle size distribution histograms, illustrating the uniformity and dispersion of particle sizes, are shown in Fig. 3g–i.

Energy dispersive X-ray (EDAX) studies

The composition of the prepared Fe_2O_3 thin films was determined using EDAX, and the corresponding spectra are presented in Fig. 4. The EDAX spectrum confirms the presence of both Fe and O in all the Fe_2O_3 thin films. The atomic percentages of Fe and O were found to be 60% and 40% for the 0.05 M precursor, 47% and 53% for the 0.1 M precursor, and 43% and 57% for the 0.15 M precursor, respectively, confirming the successful formation of Fe_2O_3 thin films.

Wettability studies

The wetting behavior of a solid surface in contact with water in air atmosphere is governed by the interfacial tension between the solid, liquid, and gas phases. A surface is considered wetting when the CA is less than 90°, and non-wetting when the CA exceeds 90°, which are referred to as hydrophilic and hydrophobic, respectively [29, 30]. These

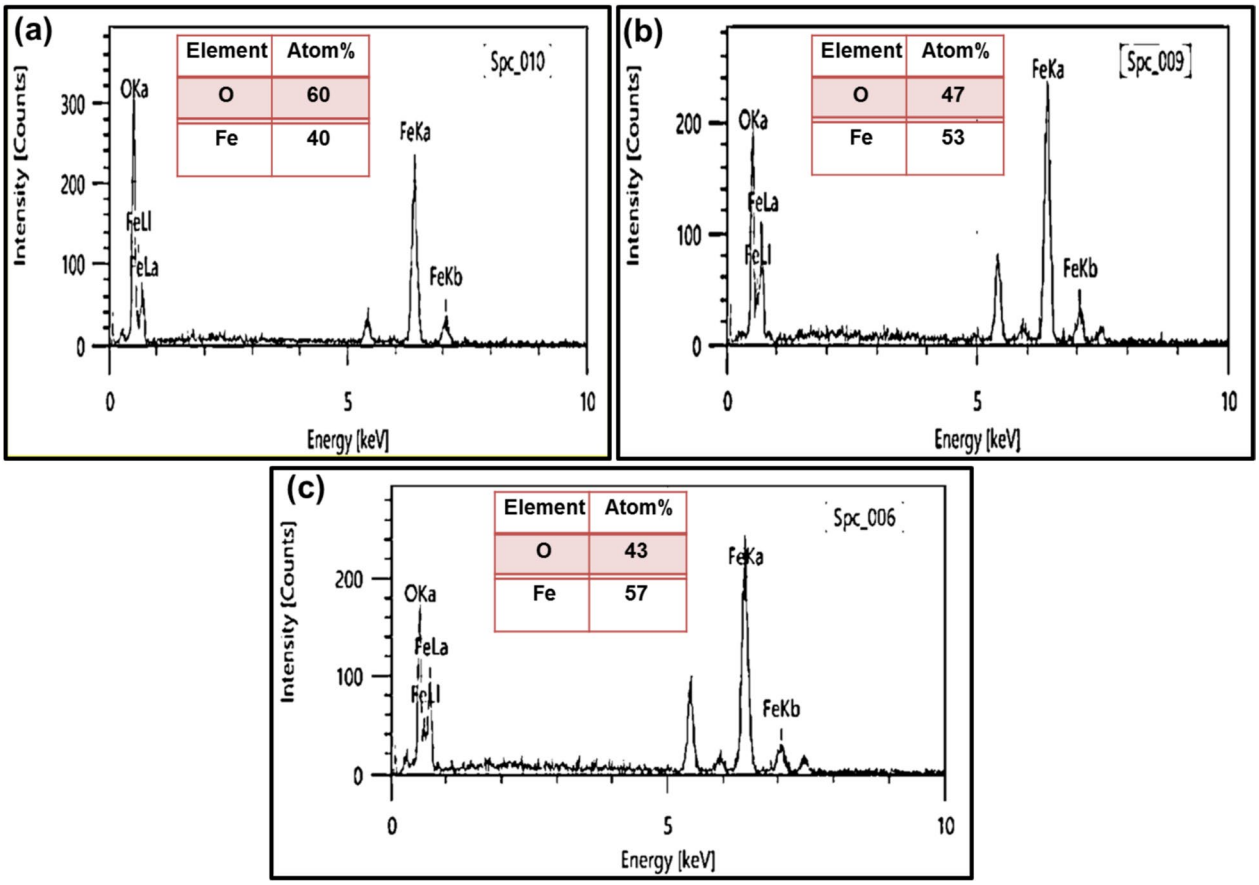

Fig. 4 EDAX spectrum of Fe_2O_3 thin film electrodes deposited at **a)** 0.05 M, **b)** 0.1 M, and **c)** 0.15 M iron precursor concentrations

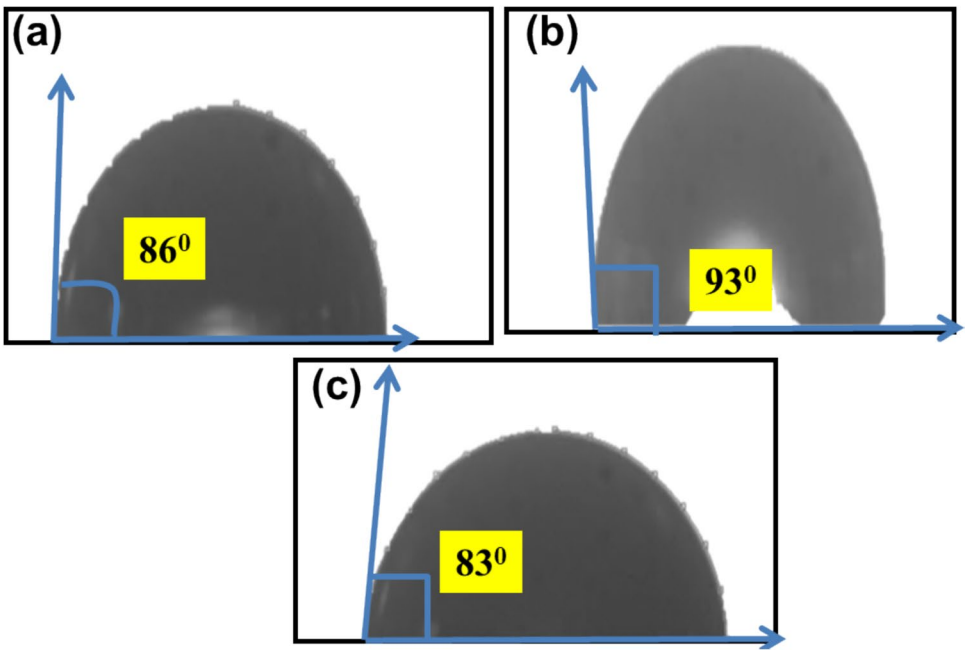

Fig. 5 Contact angle of thin films deposited at various molarity concentrations of iron precursors **a)** 0.05 M, **b)** 0.1 M, and **c)** 0.15 M

two conditions, superhydrophilic and superhydrophobic surfaces, are of significant interest in aqueous electrochemical properties. Figure 5 presents the water contact angle images of the deposited Fe_2O_3 thin films for precursor concentrations of 0.05 M, 0.1 M, and 0.15 M. In the present study, it was observed that the water contact angle increased with precursor concentrations of 0.05 M and 0.1 M. However, at a 0.15 M precursor concentration, the contact angle decreased. This behavior is attributed to an increase in film thickness up to 0.1 M concentration, followed by a decrease in thickness at 0.15 M. The lower contact angle observed at 0.15 M suggests stronger cohesive forces between water and the hydroxyl (−OH) groups present on the Fe_2O_3 thin film, indicating a more hydrophilic surface. This hydrophilic nature enhances the uniform dispersibility and electrolyte affinity of the Fe_2O_3 electrode in water, resulting in lower ion transfer resistance [31]. As a result, the dense electrode structure offers higher capacitance, and the lower contact angle is associated with reduced series resistance and improved charge transfer properties. Consequently, the energy storage performance of electrodes is enhanced by the hydrophilic nature of the electrode surface.

Surface area and porosity analysis

The surface area and pore size distribution of the material prepared using a 0.15 M iron precursor were measured, and the corresponding N_2 sorption isotherms with pore size distribution are shown in Fig. 6. According to the IUPAC classification, a hysteresis loop of type H3 was observed, with a BET surface area of 41.19 $m^2\ g^{-1}$ and a noticeable pore size distribution of 17.45 nm, as determined from BJH desorption analysis. The large specific surface area and mesoporous nanostructures provide a high number of active sites for electrolyte interaction, facilitating efficient charge transfer [32, 33].

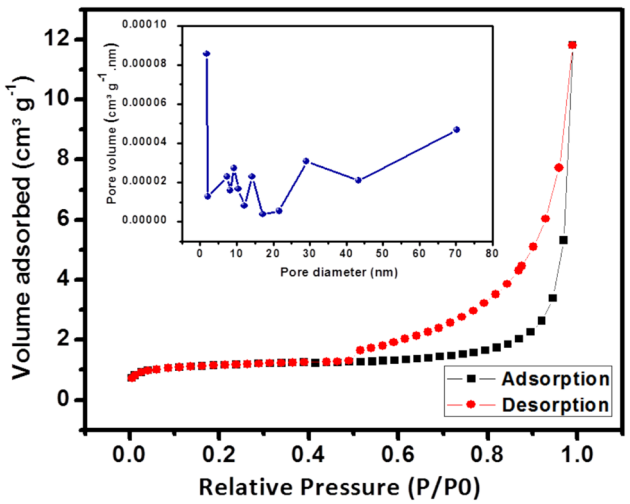

Fig. 6 N_2 sorption curve of Fe_2O_3 prepared using 0.15 M iron precursor. The inset shows BJH pore size distribution curve

Electrochemical analysis

In supercapacitor characterisations, Fe_2O_3 thin films deposited at different concentrations of iron precursors were tested using CV in 1 M NaOH electrolyte at potential range − 1.2 to − 0.4 V vs. Ag/AgCl. Comparative CV curves for all electrodes at the scan rate of 5 mV s^{-1} are shown in Fig. 7a. The CV curves show well defined redox peaks showing pseudocapacitive characteristics of the material. In the CV curves, broad redox peaks are observed around − 1.05 V and − 0.7 V vs. Ag/AgCl for all electrodes, suggesting a potential redox transition between Fe^{2+} and Fe^{3+}. The electrode with a 0.15 M iron precursor demonstrates a higher current response, indicating enhanced charge storage capacity, likely due to its lower contact angle and superior crystalline nature. As the scan rate is increased, the anodic peak shifts toward a more positive potential, while the cathodic peak shifts to a more negative potential. This behavior is consistent with the known diffusion limitations of the electrolyte ions, which result in a decrease in specific capacitance at higher scan rates [34, 35].

At lower scan rates, the ions in the electrolyte have sufficient time to diffuse and undergo charge transfer at the electrode interface, leading to an increase in specific capacitance. The specific capacitance of prepared electrodes was estimated using the following relations [36].

$$C = \frac{\int_{V0}^{V1} i(V)dV}{{}^{dv}/_{dt}\,(V_1 - V_0)} \tag{7}$$

$$\text{Specific capacitance} = \frac{C}{m} \tag{8}$$

where $\int_{V0}^{V1} i(V)dV$ area under the curve in AV, V_1 is the upper limit of the potential window and V_0 is the lower limit of the potential window, dv/dt is scan rate in V s^{-1}, C is capacitance measured in F, and m is mass of material in grams.

Figure 7e illustrates the variation of specific capacitance with scan rate for all the prepared thin film electrodes. The electrode synthesized with a 0.15 M iron precursor exhibited the highest specific capacitance. For this electrode, the specific capacitance values at scan rates of 5, 10, 20, 40, 60, 80, and 100 mV s^{-1} were 495, 374, 257, 186, 152, 132, and 118 F g^{-1}, respectively. In contrast, the specific capacitance values for the electrodes prepared with 0.05 M and 0.1 M iron precursors were 335 and 212 F g^{-1}, respectively, both lower than that of the 0.15 M precursor. The observed highest specific capacitance for the

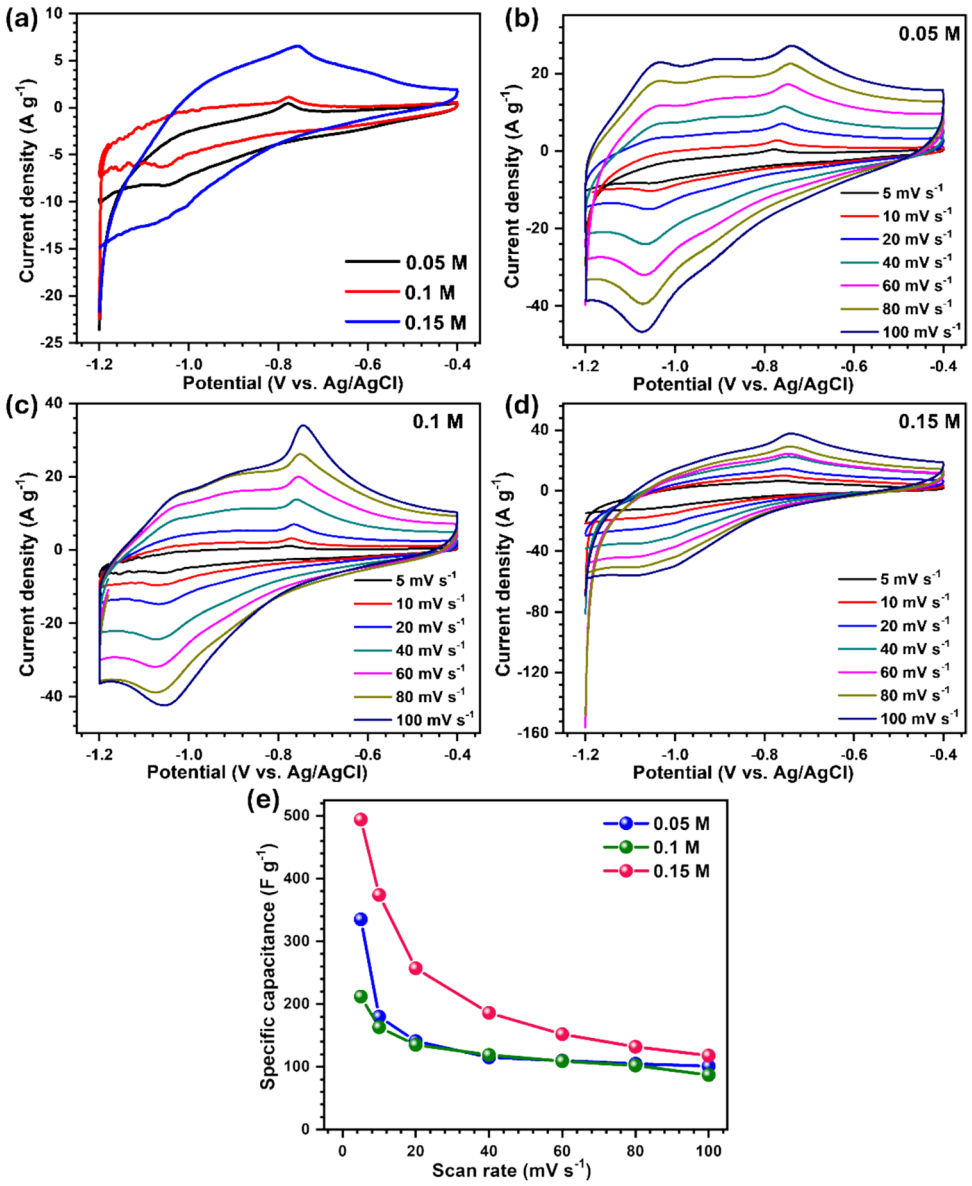

Fig. 7 **a)** Comparative CV curves of all Fe_2O_3 electrodes measured at 5 mV s^{-1}, CV curves of Fe_2O_3 electrodes prepared using iron precursor of **b)** 0.05 M, **c)** 0.1 M, **d)** 0.15 M at various scan rates ranging from 5 mV s^{-1} to 100 mV s^{-1}, and **e)** variation of specific capacitance with the scan rate for all Fe_2O_3 electrodes studied

Table 2 Electrochemical performance comparison with iron oxide-based electrodes reported in previous literature

Sr. No	Electrode	Electrolyte	Specific capacitance (F g^{-1})	Scan rate (mV s^{-1})	References
1	α-Fe_2O_3@CeO_2	2 M Na_2SO_4	168	5	[4]
2	Fe_2O_3	2 M KOH	251.5	5	[10]
3	Ppy@Fe_2O_3	0.5 M Na_2SO_4	560	5	[16]
4	α-Fe_2O_3	1 M KOH	140	10	[22]
5	RGO@Fe_3O_4	1 M KOH	771.3	5	[37]
6	Fe_2O_3	1 M KOH	218.49	5	[42]
7	Fe_2O_3	1 M NaOH	495	5	Present work

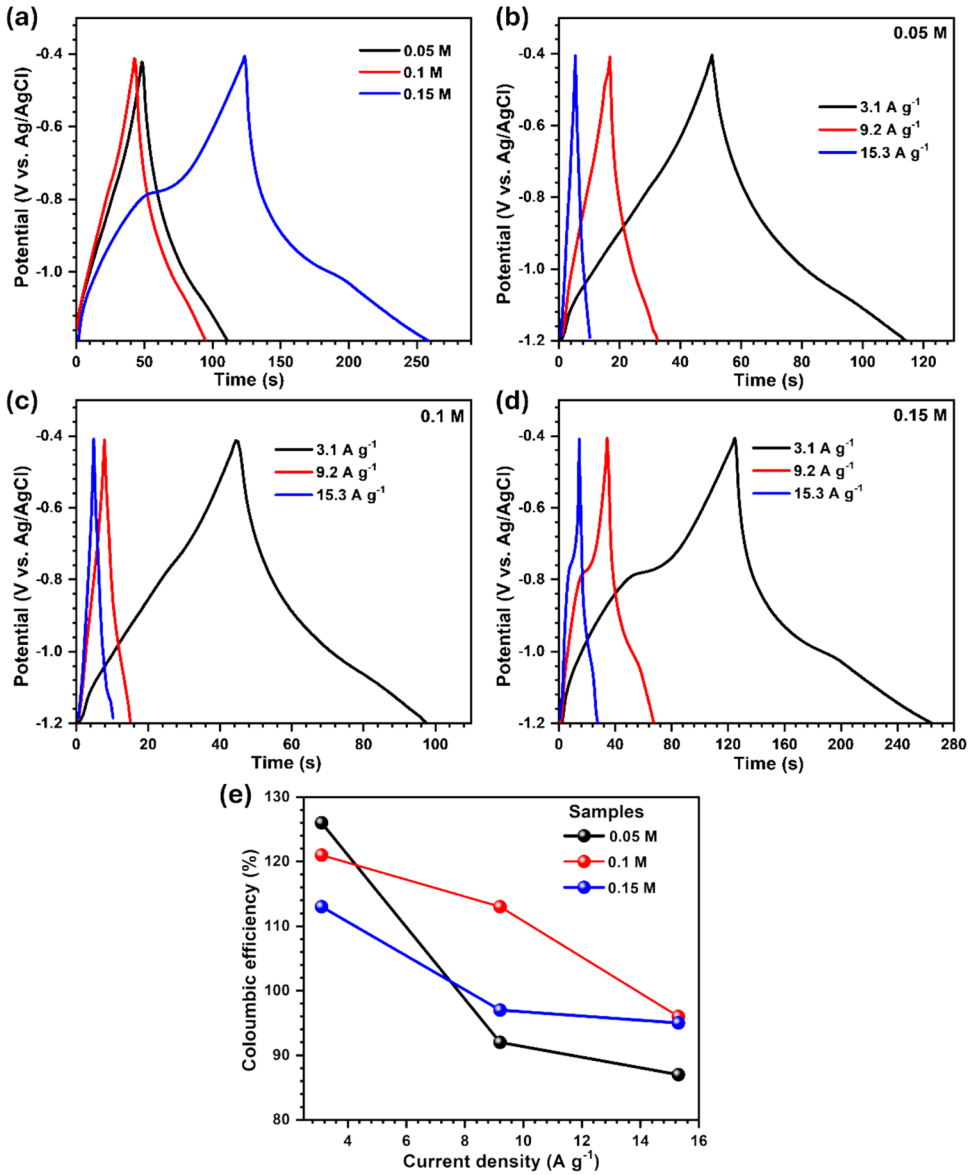

Fig. 8 **a)** Comparative GCD profiles of all Fe_2O_3 electrodes measured at 3.1 A g^{-1} current density, GCD curve of Fe_2O_3 electrodes at different current densities prepared using iron precursor of **b)** 0.05 M, **c)** 0.1 M, **d)** 0.15 M, and **e)** Coloumbic efficiency vs. current density plot

0.15 M precursor electrode is comparable to the recently reported values for iron oxide-based electrodes (Table 2).

Furthermore, to evaluate the specific capacitance, the GCD study was employed and the resulting profiles for all electrodes are shown in Fig. 8a-d. The nature of the GCD profiles indicates pseudocapacitive behaviour of the material in 1 M NaOH electrolyte. From GCD profiles measured at 3.1 A g^{-1}, we observed that the 0.15 M electrode displays higher charge–discharge time compared to other prepared electrodes, indicating higher charge storage capacity. The values of specific capacitance of all Fe_2O_3 electrodes from the GCD curves are calculated using the following equation [37],

$$\text{Specific capacitance} = \frac{i \times t_d}{V \times m} \tag{9}$$

here t_d is the discharge time, m is the mass loading, and i is the discharge current density. The highest value of specific capacitance obtained from the GCD curve is 337 F g^{-1} for 0.15 M film and 137 F g^{-1} for 0.05 M, and 102 F g^{-1} for 0.1 M electrodes at 3.1 A g^{-1} current density. The variation of specific capacitance with the current densities is shown in Fig. 8e. At lower current density, due to the highest possible utilization of the electrode material, the highest specific capacitance was observed [38, 39]. Additionally, Table 3 shows Specific and areal capacitance of all Fe_2O_3

Table 3 Specific and areal capacitance of all Fe_2O_3 electrodes prepared using iron precursors of 0.05 M, 0.1 M, and 0.15 M

Electrode	Specific capacitance (F g^{-1}) at 5 mV s^{-1}	Areal capacitance (F cm^{-2}) at 5 mV s^{-1}	Specific capacitance (F g^{-1}) at 3.1 A g^{-1}	Areal capacitance (F cm^{-2}) at 3.1 A g^{-1}
0.05 M Fe_2O_3	335	0.097	137	0.039
0.1 M Fe_2O_3	212	0.070	102	0.033
0.15M Fe_2O_3	495	0.129	337	0.088

electrodes prepared using iron precursors of 0.05 M, 0.1 M, and 0.15 M.

The Coloumbic efficiency (η) was calculated from the relation stated as follows [40]:

$$\eta = \frac{t_d}{t_c} \times 100 \tag{10}$$

where t_d and t_c are the discharging time and charging time, respectively.

The supercapacitive charge storage mechanism can be primarily classified into two types: the first being the electric double-layer charge storage mechanism, which is responsible for charge accumulation at the electrode–electrolyte interface, and the second being the diffusion-controlled mechanism, which governs charge storage through ion

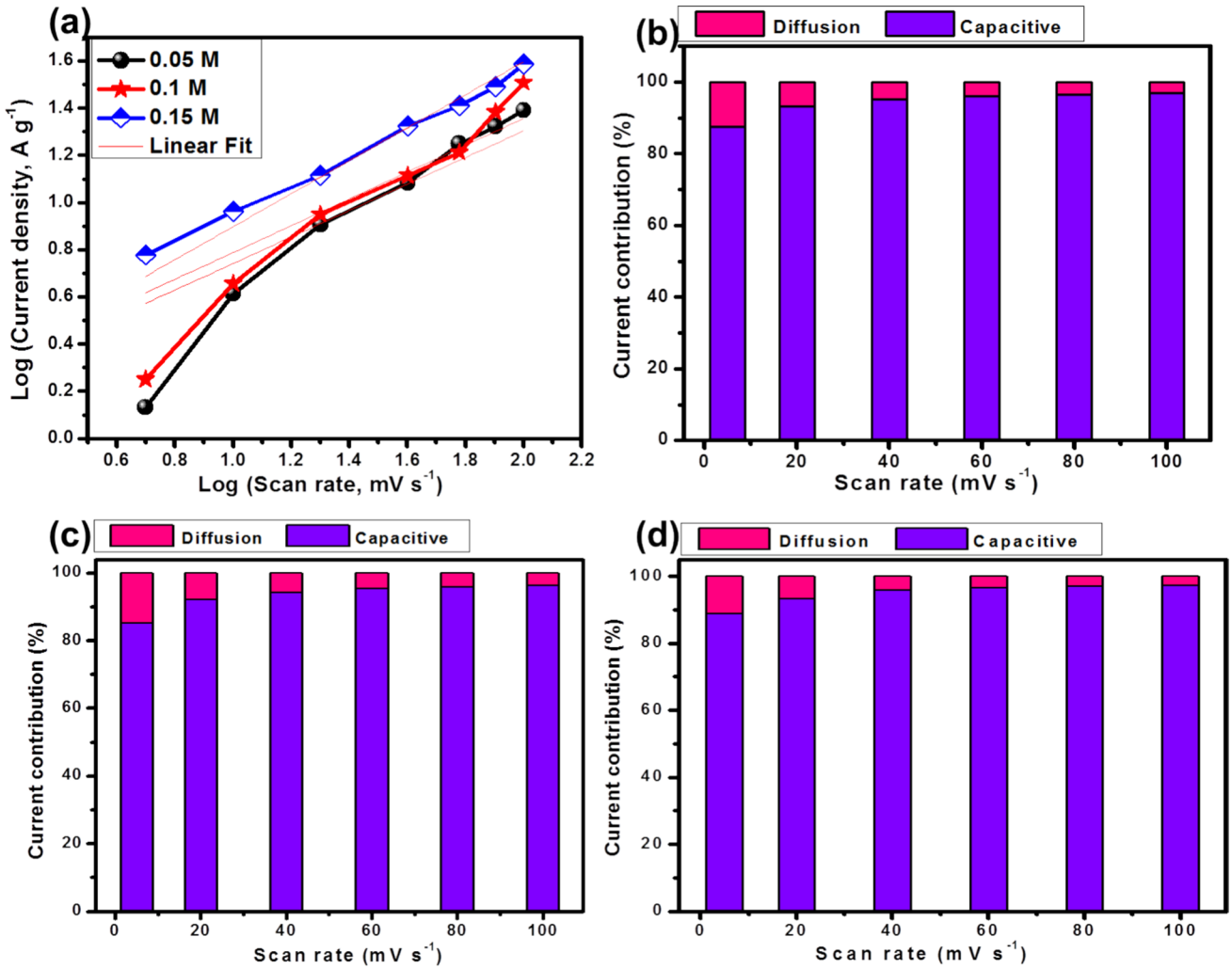

Fig. 9 **a)** Plots of log *i* and log υ, and current contribution out of total charge storage from surface-governed and diffusion-governed mechanisms at different scan rates for **b)** 0.05 M, **c)** 0.1 M, **d)** 0.15 M electrodes

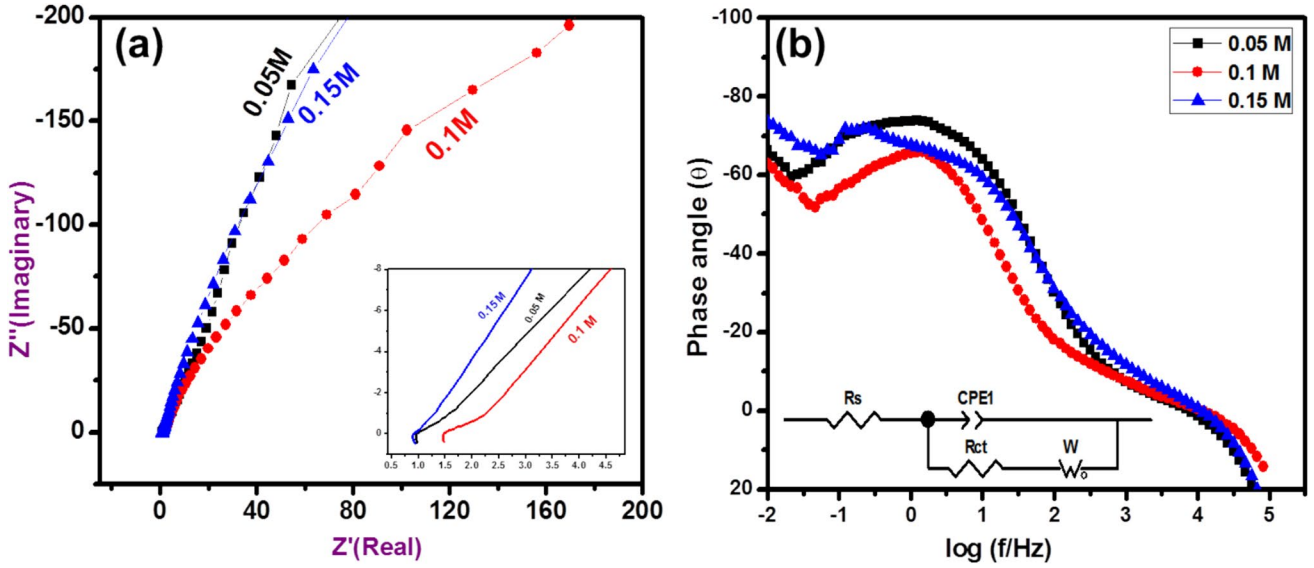

Fig. 10 (**a**) Nyquist plots of 0.05, 0.1 and 0.15 M Fe_2O_3 thin films, **b**) Bode plots for all Fe_2O_3 electrodes

diffusion [41, 42]. By applying the power law Eq. (11), the recorded current in the CV curves has a relation with the scan rate as follows [43]:

$$i_p = av^b \tag{11}$$

here a and b are the adjustable parameters, and b takes values between 0.5 to 1 depending on the charge storage mechanism. The value of b indicates whether the charge storage mechanism is primarily capacitive or diffusion-controlled [44]. For a capacitive-controlled reaction, the value of b is 1, while for a diffusion-controlled reaction, the value of b is 0.5. The calculated b-value for the optimised 0.15 M electrode is 0.69. To further quantify the contributions of capacitive and diffusion-controlled currents to the total charge storage, Eq. (12) was employed,

$$i = k_1 + k_2\sqrt{v} \tag{12}$$

The calculated capacitive contribution of the 0.15 M electrode is shown in Fig. 9b. The capacitive current contribution is 97.18 at a 100 mV s^{-1} scan rate, which reveals that the charge storage mechanism is capacitive [45].

Estimating the charge transfer resistance and phase angle, EIS measurements were performed in the frequency range of 1 MHz to 0.01 Hz. Figure 10a shows a comparative Nyquist plot for all prepared Fe_2O_3 electrodes in 1 M NaOH electrolyte. The intersection with the X-axis at the higher frequency region gives the solution resistance and the intrinsic resistance of the electrode material. The semicircle observed in the higher frequency region shows charge transfer resistance and associated double layer capacitance during the charge transfer between electrolyte and electrode, while from low frequency region, the diffusion probability is obtained [46, 47]. The EIS analysis has provided the values of R_s for 0.05, 0.1, 0.15 M electrodes are 0.97, 1.45, and 0.91 Ω, respectively. The

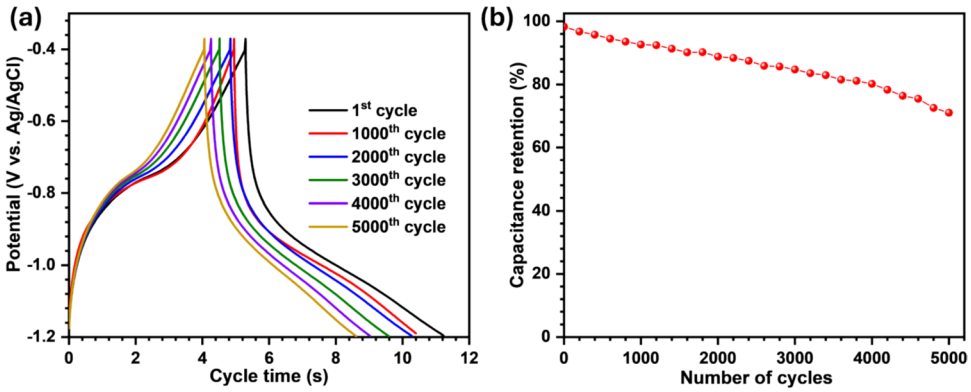

Fig. 11 **a**) GCD curves for 0.15 M Fe_2O_3 thin film electrode at different cycles, **b**) capacitance retention plot for 0.15 M Fe_2O_3 thin film electrode over 5000 GCD cycles

equivalent electronic circuit presented in Fig. 10b (see inset) is selected for fitting the obtained electrochemical impedance spectra for all Fe_2O_3 electrodes. Estimated values of R_{ct} values for 0.05, 0.1, and 0.15 M electrodes are 0.557, 1.093, and 0.440 Ω, respectively. The inclined line, making an angle of 45° in the lower frequency region, indicates Warburg impedance (*W*), characteristics of diffusion of ions between electrode materials [48].

Relaxation time constant (τ) was calculated using following expression below [49]:

$$\Gamma = \frac{1}{(2\pi f)} \tag{13}$$

where Γ is relaxation time measured in seconds, f is the frequency at the highest imaginary (Z") part of the semicircle measured in Hz. The Γ was 15 ms, which reveals a lower relaxation time constant, confirming that the electrode can be able to deliver the higher power density [50, 51]. Figure 10b shows Bode plots of Fe_2O_3 electrodes for three different molarity concentrations. The phase angle of the Fe_2O_3 electrodes is between 63° and 75° at lower frequencies, which corresponds to the contribution of capacitance from pseudocapacitance. The electrode fabricated using the 0.15 M precursor exhibits a finer and more uniform particle morphology, as observed in SEM analysis. The smaller particle size contributes to an increased electrochemically active surface area, offering more sites for charge storage. Additionally, the thinner film associated with the 0.15 M sample provides a more favourable ion diffusion path, thereby reducing internal resistance and enhancing ion accessibility to active sites. Moreover, the 0.15 M electrode displays the lowest R_{ct} and superior electrochemical conductivity.

The electrochemical stability study of the prepared electrode was very important for the practical applicability of the electrode. The stability of 0.15 M Fe_2O_3 electrode was measured over 5000 GCD cycles recorded at 15.3 A g^{-1} current density. The change in the GCD curve with the increasing cycle number was observed, indicating a decrease in the charge storage capacity. Figure 11a shows GCD curves obtained for the 1 st, 1000th, 2000th, 3000th, 4000th, and 5000th cycles. In Fig. 11b, the GCD stability shows an excellent capacity retention of 71% for 0.15 M Fe_2O_3 electrode after 5000 cycles.

Conclusion

In conclusion, self-supported Fe_2O_3 thin film electrodes were successfully deposited on SS substrates using the CBD method. The impact of precursor molarity concentration on the development and electrochemical properties of the electrode was investigated. The XRD analysis confirmed the hematite (Fe_2O_3) phase of the thin films material. The SEM images revealed irregularly shaped, randomly sized particles that were interconnected. Additionally, the EDAX confirmed the presence of iron and oxygen within the films. The 0.15 M Fe_2O_3 thin film electrode demonstrated a superior specific capacitance of 495 F g^{-1} and excellent stability, retaining 75% of its initial capacitance after 1000 cycles, owing to its 41.19 m^2 g^{-1} specific surface area and self-supported nature. These findings highlight the potential of Fe_2O_3 thin films for high-performance supercapacitor applications.

Acknowledgements The authors gratefully acknowledge the Prof. C. D. Lokhande Endowment Charitable Trust, Kolhapur, for financial support.

Author contributions A. A. Admuthe: Conceptualization, Methodology, Investigation, Data curation and manuscript writing. P. A. Desai: Resources, Formal analysis. S. G. Pawar: Electrochemical measurements of prepared sample. S. L. Jadhav: Modification, Creation, Presentation, Visualization. A. L. Jadhav: Modification, Creation, and Presentation D. B. Malavekar: Resources, manuscript review and editing. N. S. Bachankar: Presentation, J. H. Kim: Resources. K. V. Gaikwad: Visualization, Validation. V. S. Jamadade: Modification, Creation, Presentation, Visualization, Supervision and Manuscript editing.

Data availability Data will be made available on request.

Declarations

Competing interest The authors declare no competing interests.

References

1. Youssry S, El-Nahass M, Kumar R, El-Hallag I, Tan W, Matsuda A (2020) Superior performance of $Ni(OH)_2$-ErGO@ NF electrode materials as pseudocapacitance using electrochemical deposition via two simple successive steps. J Energy Storage 30:101485. https://doi.org/10.1016/j.est.2020.101485
2. Ghalmi Y, Habelhames F, Sayah A, Bahloul A, Nessark B, Shalabi M, Nunzi J (2019) Capacitance performance of NiO thin films synthesized by direct and pulse potentiostatic methods. Ionics 25:6025–6033. https://doi.org/10.1007/s11581-019-03159-2
3. Tounsi A, Sayah A, Lamiri L, Boumaza N, Habelhames F, Bahloul A, Chenni C, Nessark B, Saeed M (2023) One-step electrochemical synthesis of FTO/MnO_2-graphene composite for electrochemical energy storage. J Energy Storage 73:109228. https://doi.org/10.1016/j.est.2023.109228
4. Sayah A, Bahloul A, Habelhames F, Boumaza N, Ghalmi Y, Tounsi A, Lamiri L, Nessark B, Ghelani L, Chala A (2024) Electrodeposition mode effects on the electrochemical performance of cobalt sulfide material for supercapacitors. Ionics 31:851–864. https://doi.org/10.1007/s11581-024-05903-9
5. Houssou A, Amirat S, Bouchelaghem W, Sayah A, Ferkous H, Rehamnia R (2024) Effect of morphology on the electrochemical performance of NiO thin films. Bull Mater Sci 47:126. https://doi.org/10.1007/s12034-024-03190-8
6. Bachankar SB, Malavekar DB, Lokhande VC, Ji T (2024) Empowering supercapacitors: strategic B-site modulations of transition metal atoms in perovskite oxide based electrodes. J Alloys Compd 1003:175708. https://doi.org/10.1016/j.jallcom.2024.175708

7. Benzigar M, Joseph S, Saianand G, Gopalan A, Sarkar S, Srinivasan S, Park D, Kim S, Talapanenia S, Ramadass K, Vinu A (2019) Highly ordered iron oxide-mesoporous fullerene nano composites for oxygen reduction reaction and supercapacitor applications. MICROPOR MESOPOR MAT 285:21–31. https://doi.org/10.1016/j.micromeso.2019.04.071
8. Ardakani M, Sabaghian F, Yavari M, Ebady A, Sahraie N (2020) Enhance the performance of iron oxide nanoparticles in supercapacitor applications through internal contact of α-Fe_2O_3@CeO_2 core-shell. J Alloys Compd 819:152949. https://doi.org/10.1016/j.jallcom.2019.152949
9. Xia Q, Xu M, Xia H, Xie J (2016) Nanostructured Iron Oxide/Hydroxide-Based Electrode Materials for Supercapacitors. ChemNanoMat 2:588–600. https://doi.org/10.1002/cnma.2016.00110
10. Lakra R, Kumar R, Kumar P, Kumar S, Soam A (2022) Application of Iron Oxide in Supercapacitor, Iron Oxide Nanoparticles 180. https://doi.org/10.5772/intechopen.95129.
11. Lakra R, Mahender C, Singh B (2023) $ZnFe_2O_4$ nanoparticles supported on graphene nanosheets for high-performance supercapacitor. J Electron Mater 52:2676–2684. https://doi.org/10.1007/s11664-023-10230-2
12. Sayah A, Boumaza N, Habelhames F (2024) Electrodeposition mode effects on the electrochemical performance of MnO_2–NiO eco-friendly material for supercapacitor electrode application. J Mater Sci: Mater Electron 35:62. https://doi.org/10.1007/s10854-023-11832-6
13. Lakra R, Kumar R, Kumar S, Thatoi D, Soam A (2023) Synthesis of TiO_2 nanoparticles as electrodes for supercapacitor. Mater Today: Proc 74:863–866. https://doi.org/10.1016/j.matpr.2022.11.271
14. Elsaidy A, Majcherkiewicz JN, Puértolas B, Salgueiriño V, Nóvoa XR, Correa-Duarte MA (2022) Synergistic interaction of clusters of iron oxide nanoparticles and reduced graphene oxide for high supercapacitor performance. Nanomaterials 12(15):2695. https://doi.org/10.3390/nano12152695
15. Dhas S, Maldar P, Patil M, Nagare A, Waikar M, Sonkawade R, Moholkar A (2020) Synthesis of NiO nanoparticles for supercapacitor application as an efficient electrode material. Vacuum 181:109646. https://doi.org/10.1016/j.vacuum.2020.109646
16. Cai D, Du J, Zhu C, Cao Q, Huang L, Wu J, Zhou D, Xia Q, Chen T, Guan C, Xia Y (2020) Iron oxide nanoneedles anchored on n-doped carbon nanoarrays as an electrode for high-performance hybrid supercapacitor. ACS Appl Energy Mater 3(12):12162–12171. https://doi.org/10.1021/acsaem.0c02238
17. Aldalbahi A, Samuel E, Alotaibi B, El-Hamshary H, Yoon S (2021) Reduced graphene oxide supersonically sprayed on wearable fabric and decorated with iron oxide for supercapacitor applications. JMST 82:47–56. https://doi.org/10.1016/j.jmst.2020.11.066
18. Bera A, Maitra A, Das A, Halder L, Paria S, Si S, De A, Ojha S, Khatua B (2020) A quasi-solid-state asymmetric supercapacitor device based on honeycomb-like nickel-copper-carbonate-hydroxide as a positive and iron oxide as a negative electrode with superior electrochemical performances. ACS Appl Electron Mater 2:177–185. https://doi.org/10.1021/acsaelm.9b00677
19. Patil DJ, Malavekar DB, Lokhande VC, Bagwade PP, Khot SD, Ji T, Lokhande CD (2022) Binder-free synthesis of mesoporous nickel tungstate for aqueous asymmetric supercapacitor applications: Effect of film thickness. Energy Technol 10(8):2200295. https://doi.org/10.1002/ente.202200295
20. Bhosale R, Kumbhar S, Bhosale S, Salunkhe R, Kadam V, Pardhi S, Gholap S, Lokhande C, Jamadade V (2024) Morphology modulation of $MnFe_2O_4$ thin film electrode for enhanced performance of hybrid supercapacitor. J Energy Storage 86:111146. https://doi.org/10.1016/j.est.2024.111146
21. Sohouli E, Adib K, Maddah B, Najafi M (2022) Preparation of a supercapacitor electrode based on carbon nano-onions/manganese dioxide/iron oxide nanocomposite. J Energy Storage 52:104987. https://doi.org/10.1016/j.est.2022.104987
22. Kumar R, Youssry S, Joanni E, Sahoo S, Kawamura G, Matsuda A (2022) Microwave-assisted synthesis of iron oxide homogeneously dispersed on reduced graphene oxide for high performance supercapacitor electrodes. J Energy Storage 56:105896. https://doi.org/10.1016/j.est.2022.105896
23. Bhosale RP, Kumbhar SS, Bagwade PP, Shelke HD, Lokhande CD, Jamadade VS (2024) Chemical synthesis of manganese ferrite thin films for energy storage application. J Mater Sci: Mater Electron 35(1):5. https://doi.org/10.1007/s10854-023-11706-x
24. Xu C, Rafael A, Santiago P, Padron D, Caballero A, Balu A, Romero A, Batista MM, Luque R (2019) Controllable design of polypyrrole-iron oxide nanocoral architectures for supercapacitors with ultrahigh cycling stability. Appl Energy Mater 2:2161–2168. https://doi.org/10.1021/acsaem.8b02167
25. Hassanien A, Akl A (2018) Optical characteristics of iron oxide thin films prepared by spray pyrolysis technique at different substrate temperatures. Appl Phys A 124:752. https://doi.org/10.1007/s00339-018-2180-6
26. Kunhikrishnan L, Shanmugham R (2021) High electrochemical performance of morphologically controlled cobalt oxide for supercapacitor application. Mater Charact 177:111160. https://doi.org/10.1016/j.matchar.2021.111160
27. Jadhav S, Jadhav A, Mandlekar B, Sarawade P, Kadam A (2023) Influence of deposition curret and different electrolytes on charge storage performance of Co_3O_4 electrode material. J Phys Chem Solids 180:111422. https://doi.org/10.1016/j.jpcs.2023.111422
28. Malavekar D, Pujari S, Jang S, Bachankar S, Kim JH (2024) Recent development on transition metal oxides-based core-shell structures for boosted energy density supercapacitors. Small 20(31):2312179. https://doi.org/10.1002/smll.202312179
29. Malavekar D, Pawar D, Bagde A, Khot S, Sankapal S, Bachankar S, Patil S, Lokhande C, Kim J (2024) Advancements in graphene and its derivatives based composite Materials: A comprehensive review on Synthesis, Characterization, and supercapacitive charge storage. Chem Eng J 501:157533. https://doi.org/10.1016/j.cej.2024.157533
30. Malavekar DB, Kale SB, Lokhande VC, Patil UM, Kim JH, Lokhande CD (2020) Chemically synthesized Cu_3Se_2 film based flexible solid-state symmetric supercapacitor: Effect of reaction bath temperature. J Phys Chem C 124(52):28395–28406. https://doi.org/10.1021/acs.jpcc.0c08454
31. Qureshi AA, Javed S, Javed HMA, Jamshaid M, Ali U, Akram MA (2022) Systematic investigation of structural, morphological, thermal, optoelectronic, and magnetic properties of high-purity hematite/magnetite nanoparticles for optoelectronics. Nanomaterials 12(10):1635. https://doi.org/10.3390/nano12101635
32. Qayoom M, Shah K, Pandit A, Firdous A, Dar G (2020) Dielectric and electrical studies on iron oxide (α-Fe_2O_3) nanoparticles synthesized by modified solution combustion reaction for microwave applications. J Electroceram 45:7–14. https://doi.org/10.1007/s10832-020-00219-2
33. Jiang K, Sun B, Yao M, Wang N, Hu W, Komarneni S (2018) In situ hydrothermal preparation of mesoporous Fe_3O_4 film for high-performance negative electrodes of supercapacitors. Micropor Mesopor Mat 265:189–194. https://doi.org/10.1016/j.micromeso.2018.02.015
34. Fouad D, Zhang C, El-Didamony H, Yingnan L, Mekuria T, Shah A (2019) Improved size, morphology and crystallinity of hematite (α-Fe_2O_3) nanoparticles synthesized via the precipitation route using ferric sulfate precursor. Results Phys 12:1253–1261. https://doi.org/10.1016/j.rinp.2019.01.005

35. Lassoued A, Dkhil B, Gadri A, Ammar S (2017) Control of the shape and size of iron oxide (α- Fe_2O_3) nanoparticles synthesized through the chemical precipitation method. Results Phys 7:3007–3015. https://doi.org/10.1016/j.rinp.2017.07.066
36. Wang P, Zhang X, Duan W, Teng W, Liu Y, Xie Q (2021) Superhydrophobic flexible supercapacitors formed by integrating hydrogel with functional carbon nanomaterials. Chin J Chem 39:1153–1158. https://doi.org/10.1002/cjoc.202000543
37. Yadav A, Hunge Y, Seongjun K, Seok-Won K (2022) Chemically synthesized iron-oxide-based pure negative electrode for solid-state asymmetric supercapacitor devices. Materials 15:6133. https://doi.org/10.3390/ma15176133
38. Jadhav S, Jadhav A, Kadam A (2022) Porous crosslinked Co_3O_4 nanoflakes synthesized at different pH media for electrochemically charge storage applications. Electrochim Acta 426:140845. https://doi.org/10.1016/j.electacta.2022.140845
39. Li Y, Meng Y, Xiao M, Liu X, Zhu F, Zhang Y (2019) The surface capacitance behavior and its contribution to the excellent performance of cobalt ferrite/carbon anode in lithium storage. J Mater Sci: Mater Electron 30:12659–12668. https://doi.org/10.1007/s10854-019-01629-x
40. Jadhav SL, Jadhav AL, Sarawade PB, Mandlekar BK, Kadam AV (2024) Mo-doped porous Co_3O_4 nanoflakes as an electrode with the enhanced capacitive contribution for asymmetric supercapacitor application. J Energy Stor 82:110540. https://doi.org/10.1016/j.est.2024.110540
41. Sagadevan S, Marlinda A, Umar A, Foud H, Alothman O, Khaled U, Akhtar M, Shahid M (2020) Reduced graphene/ nanostructured cobalt oxide nanocomposite for enhanced electrochemical performance of supercapacitor applications. J Colloid Interface Sci 558:68–77. https://doi.org/10.1016/j.jcis.2019.09.081
42. Du F, Zuo X, Yang Q, Li G, Ding Z, Wu M, Jin S, Zhu K (2016) Facile hydrothermal reduction synthesis of porous Co_3O_4 nanosheets @RGO nanocomposite and applied as a supercapacitor electrode with enhanced specific capacitance and excellent cycle stability. Electrochim Acta 222:976–982. https://doi.org/10.1016/j.electacta.2016.11.065
43. Zhou J, Xu S, Ni L, Chen N, Li X, Lu C, Wang X, Peng L, Guo X, Ding W, Hou W (2019) Iron oxide encapsulated in nitrogen-doped carbon as high energy anode material for asymmetric supercapacitors. J Power Sources 438:227047. https://doi.org/10.1016/j.jpowsour.2019.227047
44. Javed M, Khan A, Hanif M, Nazir M, Hussain S, Saleem M, Raza R, Yung S, Liu Z (2021) Engineering the performance of negative electrode for supercapacitor by polyaniline coated Fe_3O_4 nanoparticles enables high stability up to 25,000 cycles. Int J Hydrogen Energy 46:9976–9987. https://doi.org/10.1016/j.ijhydene.2020.04.173
45. Chen L, Liu D, Yang P (2019) Preparation of α-Fe_2O_3/rGO composites toward supercapacitor applications. RSC Adv 9:12793. https://doi.org/10.1039/C9RA01928F
46. Kumar R, Youssry S, Ya K (2020) Microwave-assisted synthesis of Mn_3O_4- Fe_2O_3/Fe_3O_4@rGO ternary hybrids and electrochemical performance for supercapacitor electrode. Diam Relat Mater 101:107622. https://doi.org/10.1016/j.diamond.2019.107622
47. Khatavkar S, Sartale S (2019) α-Fe_2O_3 thin film on stainless steel mesh: A flexible electrode for supercapacitor. Mater Chem Phys 225:284–291. https://doi.org/10.1016/j.matchemphys.2018.12.079
48. Zuo W, Zang L, Wang X, Liu Q, Qiu J, Liang C, Liu X, Yang C (2020) Flexible Polypyrrole@Fe_2O_3@Stainless steel yarn composite electrode for symmetric thread-like supercapacitor with extended operating voltage window in Li_2SO_4-based aqueous electrolyte. Adv Sustain Syst 4:2000173. https://doi.org/10.1002/adsu.202000173
49. Orisekeh K, Singh B, Olanrewaju Y, Kigozi M, Ihekweme G, Umar S, Anye V, Bello A, Parida S, Soboyejo WO (2021) Processing of α-Fe_2O_3 nanoparticles on activated carbon cloth as binder-free electrode material for supercapacitor energy storage. J Energy Storage 33:102042. https://doi.org/10.1016/j.est.2020.102042
50. Phakkhawan A, Suksangrat P, Srepusharawoot P, Ruangchai S, Klangtakai P, Pimanpang S, Amornkitbamrung V (2022) Reagent-and solvent-mediated Fe_2O_3 morphologies and electrochemical mechanism of Fe_2O_3 supercapacitors. J Alloys Compd 919:165702. https://doi.org/10.1016/j.jallcom.2022.165702
51. Khedulkar A, Yu W, Dang V, Pandit B, Doong R (2024) Boosting supercapacitor performance with a cobalt hydroxide in situ preparation orange peel biochar flower-like composite. J Energy Storage 81:110302. https://doi.org/10.1016/j.est.2023.110302